International Journal of Earth Sciences (2018) 107:2539–2552
https://doi.org/10.1007/s00531-018-1613-y

ORIGINAL PAPER

SHRIMP U–Pb detrital zircon dating to check subdivisions in metamorphic complexes: a case of study in the Nevado–Filábride complex (Betic Cordillera, Spain)

Ángel Santamaría-López[1] · Carlos Sanz de Galdeano[2]

Received: 22 November 2017 / Accepted: 18 April 2018 / Published online: 26 April 2018

Abstract
U–Pb dating on inherited detrital zircons has been applied to obtain the probable maximum age of deposition of the detrital protolith of the Nevado–Filábride complex (Betic Cordillera, Spain). Five of eight samples correspond to the lower part of the lithologic sequence of this complex, where radiometric dating of metasediments has not been presented till the present. The youngest age populations in the majority of samples are Carboniferous. The estimation of the maximum age of deposition in the lower and upper units is 349.1 ± 1.6 and 334.6 ± 2.9 Ma, respectively. In addition, samples show common age populations at ca. 490–630 and ca. 910–1010 Ma. Observations agree with the Carboniferous to early Permian U–Pb ages previously obtained in orthogneisses levels which are situated in the upper part of the complex. Combination of the minimum age of deposition deducible from the orthogneisses studies and the maximum ages of deposition obtained from the detrital zircons of this work, allow establishing the deposition of de studied lithological succession comprised between ca. 282 and 349 Ma or a shorter period.

Keywords U–Pb geochronology · Detrital zircons · SHRIMP · Nevado–Filábride complex · Betic Cordillera

Introduction

An essential topic in the study of lithological successions is the determination of the age of rocks which yield geologists to a better understanding of the formation and evolution of the stratigraphic sequences. Paleontological approach is one of the primary tools to determinate the age of the rocks. But in absence of fossils, as usually occurs in metamorphic and igneous rocks, age determinations based on radiometric dating methods are usually implemented in the studies.

U–Pb geochronology applied to zircon is widely use to estimate probable age constrains in lithological successions due to the remarkable resistance of zircon grains to deformation and metamorphism, and the consequent abundance of this mineral in sedimentary and metamorphic rocks (e.g., Dickinson and Gehrels 2009; Díez-Fernández et al. 2010; Fedo et al. 2003; Gehrels 2012, 2014; Litty et al. 2017; Meinhold et al. 2013; Pérez-Cáceres et al. 2017; Schoene 2014; Thomson et al. 2017). In particular in sedimentary and metamorphic successions, dating of inherited detrital zircons can be used to determinate the most likely maximum age of deposition (MDA) of the detrital protolith. This interpretation is based on the identification of the youngest age population and requires a large number of samples to ensure the results to be statistically representative (e.g., Andersen 2005; Fedo et al. 2003; Gehrels 2012). Therefore, ion microprobe (SIMS) and Laser Ablation Inductively Coupled Plasma Mass Spectrometry (LA-ICPMS), which permit the analysis of large number of zircon grains (see Davis et al. 2003; Fedo et al. 2003; Kosler and Sylvester 2003 for a historical review of

Electronic supplementary material The online version of this article (https://doi.org/10.1007/s00531-018-1613-y) contains supplementary material, which is available to authorized users.

✉ Ángel Santamaría-López
angelsan83@correo.ugr.es

Carlos Sanz de Galdeano
csanz@ugr.es

[1] Departamento de Química Inorgánica, Cristalografía y Mineralogía, Facultad de Ciencias, Universidad de Málaga, 29071 Málaga, Spain

[2] Instituto Andaluz de Ciencias de la Tierra, Consejo Superior de Investigaciones Científicas-Universidad de Granada, Facultad de Ciencias, 18071 Granada, Spain

the methods), constitute the best analytical instruments to determinate the most probable MDAs. The determination of age populations in samples from different lithologic sequences allow comparison between them, and provide results useful to verify or reject proposed subdivisions which have been previously based on lithological and tectonic criteria (e.g., Kirkland et al. 2008; Rónadh et al. 2004).

The sedimentary age estimations of the Nevado–Filábride complex in the Sierras Nevada and Filabres (Betic Cordillera, Spain) (Fig. 1) are traditionally based on stratigraphic correlations with the overlying Alpujárride complex (see the geological setting below), and show a Paleozoic (and even older) lower sequence, and a Permo-Triassic cover (e.g., Egeler and Simon 1969). In addition, the deposition of carbonates in the upper part of the Nevado–Filábride sequence (now present as marbles) has been assumed as Triassic (de Jong and Bakker 1991). Gómez-Pugnaire et al. (1982) identified possible pre-Cambrian microfossils in metapelites from the western part of the Sierra de los Filabres. However, these preliminary results have not been confirmed so far. Tendero et al. (1993) studied the northern part of this sierra and reported ankeritic "ghosts" in the higher parts of the lithological sequence that were interpreted as Cretaceous planktonic foraminifers. Recently, Rodríguez-Cañero et al. (2017), also in the Sierra de los Filabres, found Bashkirian conodonts in graphite-rich limestone levels (323.2 ± 0.4–315.2 ± 0.2 Ma) which in our interpretation are situated in upper part of the lithological sequence.

Radiometric age determinations of the complex have been mainly based on meta-igneous rocks situated in the upper part of the complex. However, the ages of the lower part of the sequence have not been determined until now. The first radiometric dating study on the Nevado–Filábride complex rocks provided Rb–Sr whole-rock age of 269 ± 6 Ma for tourmaline-gneisses and metagranites in the eastern part of Sierra de los Filabres area (Priem et al. 1966). Puga (1976) (in the western part of Sierra Nevada), Andriessen et al. (1991) (in the eastern part of the complex) and Gómez-Pugnaire et al. (2000) (in the central part of the complex) proposed Rb–Sr whole-rock ages from early Permian to Triassic for gneisses. Nieto (1996) and Nieto et al. (1997) reported an age of 307 ± 30 Ma using Sm–Nd whole-rock analyses in orthogneisses. In the western part of the Nevado–Filábride complex U–Pb age determinations include: Gómez-Pugnaire et al. (2004), who obtained late Carboniferous age from orthogneisses (301 ± 7 Ma); Martínez-Martínez et al. (2010), who proposed late Carboniferous U–Pb ages in zircons (314 ± 7 and 304 ± 23 Ma) and $^{40}Ar/^{39}Ar$ tourmaline ages in gneisses and tourmalinites (319.85 ± 5.81 and 317.85 ± 3.67 Ma); and Ruiz-Cruz and Sanz de Galdeano (2017), who gave lower Permian U–Pb ages from zircons extracted from orthogneisses (~ 286 Ma). Gómez-Pugnaire et al. (2012) determined lower Permian U–Pb zircon ages in gneisses from various areas of the complex (282 ± 5–295 ± 3 Ma).

In our opinion the study of the ages of the Nevado–Filábride lithological sequences remains incomplete because

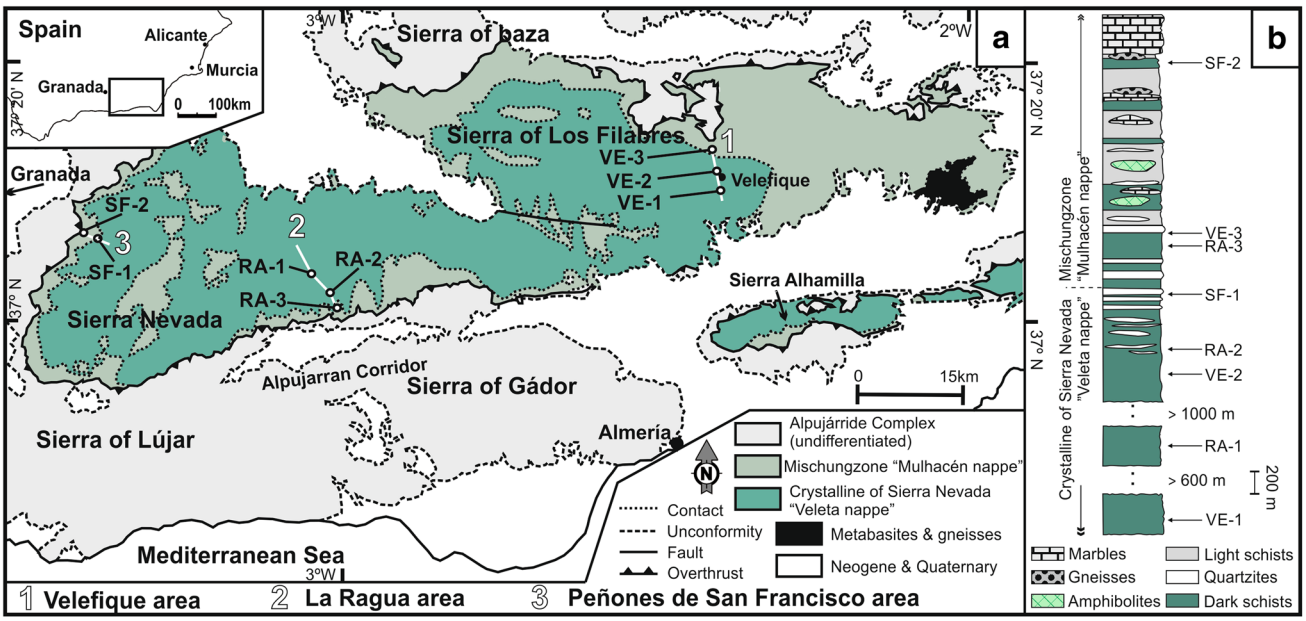

Fig. 1 Geological setting of the southeast of the Iberian Peninsula. **a** General map of the Betic cordillera showing the Nevado–Filábride complex distribution. The sampling areas: Velefique, La Ragua and Peñones de San Francisco, are shown as lines labeled as 1, 2 and 3 respectively. **b** Schematic lithological succession of the Nevado–Filábride complex

the studies based on meta-igneous rocks can only provide minimum ages of sedimentation. The dataset of detrital zircon ages is, to our knowledge, limited to a single study of a tourmaline-rich mica-schist sample situated in upper part of the lithological sequence (see Gómez-Pugnaire et al. 2012 and their sample PC-3, whose zircons yielded $^{206}Pb/^{238}U$ dates ~ 336, 700 and 2050 Ma). Therefore, to determinate a better constrained MDA for the complex it is necessary to undertake a more extensive study based on multiple samples. Besides, determination of age populations obtained in samples from different parts of the complex can be used to check the proposed subdivisions which have been traditionally based on tectonometamorphic observations (e.g., Augier et al. 2005; Behr and Platt 2012; Booth-Rea et al. 2015; de Jong 1991, 1993; Martínez-Martínez et al. 2002; Puga et al. 2002).

The Nevado–Filábride complex and the debate concerning the age and the proposed subdivisions constitute an excellent case of study for the application of U–Pb dating on detrital zircons. In the present paper we provide the results of detrital zircon U–Pb SHRIMP dating of eight schist samples from the Nevado–Filábride complex. Five of these samples were taken in the lower part of the sequence allowing, for the first time, to provide age estimates for the MDA of this part of the complex. External and internal zircon grain features have been analyzed by transmitted-light, backscattered, and cathodoluminescence (CL) images to identify crystal properties which allow interpretation of the former origin of the zircons, and to rule out the presence of metamorphic grains formed after the deposition. Ages obtained have been compared with the results based on meta-igneous rocks dating. Additionally, it has been presented a preliminary study of the inclusions found in the zircon grains based in backscattered images.

Geological setting

The Betic Cordillera, situated in the S and SE of the Iberian Peninsula (Fig. 1), constitutes, together with the Rif, the westernmost part of the Mediterranean Alpine belt. It is divided in two domains: the Internal and the External Zones (Fallot 1948). The External Zone is a Mesozoic and Tertiary age sedimentary succession deposited in the S and SE paleomargin of the Paleozoic Iberian Massif. The Internal Zone is divided into three main complexes (Fig. 1) named, from bottom to top, Nevado–Filábride, Alpujárride, and Maláguide (Egeler and Simon 1969).

The Nevado–Filábride complex was defined by Egeler (1963) and its tectonic division has been under debate since the original studies. Brouwer (1926) initially differentiated two formations mainly based in lithological differences: the lower one "Crystalline of Sierra Nevada", and the upper "Mischungszone" (or Mixed zone). The Crystalline of Sierra Nevada (Fig. 1) is formed by a monotonous Paleozoic or older succession of dark graphitic mica schists with quartzite layers. The Mischungszone (Fig. 1) has more lithological variety, and it is formed by dark and light schists, mica schists, quartzites, marbles, gneisses, serpentinites, and amphibolites. Several subdivisions have been introduced later on. Puga (1976) divided the Nevado–Filábride complex into the lowermost Veleta nappe and the Mulhacén nappe at the top, which essentially correspond to the Crystalline of Sierra Nevada and the Mischungszone, respectively. Puga et al. (2002) redefined these nappes as complexes based in tectonometamorphic criteria: the Veleta complex and the Mulhacén complex. Martínez-Martínez et al. (2002) divided the Nevado–Filábride complex into three major tectonic units called from bottom to top: Ragua, Calar-Alto, and Bédar-Macael. The subdivision proposed by Martínez-Martínez et al. (2002) and those of Puga (1976) are not completely equivalent. The Ragua unit is almost equivalent to the Veleta nappe, but in the Ragua unit the upper part of the Veleta nappe is excluded, this being named by Martínez-Martínez et al. (2002) as Montenegro dark schists. The Calar-Alto unit corresponds to the Montenegro dark schists and the lower part of the Mulhacén nappe. Finally, the Bédar-Macael unit corresponds to the higher part of the Mulhacén nappe. On the contrary, some authors, based on lithological and structural studies, do not support the division of the complex in several units, but the existence of a continuous lithological succession (e.g., Galindo-Zaldívar 1993; Monié et al. 1991; Sanz de Galdeano and López-Garrido 2016; Sanz de Galdeano et al. 2016). The Nevado–Filábride complex underwent Alpine polyphased metamorphism proposed to be Miocene (Behr and Platt 2012; Gómez-Pugnaire et al. 2004, 2012; López-Sánchez-Vizcaíno et al. 2001) or to have developed during Oligocene and Miocene (Augier et al. 2005).

Methodology

The SEM-EDX (X-ray dispersive energy) study and electron backscattered (BSE) images were made using an environmental scanning electron microscope FEI model Quanta 400, operating at 15–20 keV (Centro de Instrumentación Científica-CIC, University of Granada, Spain).

The zircon grains were separated using panning, first in water and then in ethanol, and magnetic techniques followed by handpicking of the concentrates using a binocular microscope. Once mounted and polished zircon grains were studied by optical and CL imaging and analyzed for U–Pb using a SHRIMP IIe/mc ion microprobe at the IBERSIMS laboratory of the University of Granada (Spain). SHRIMP investigations were guided by CL images to select the best

location for the analyses in the mounted zircons. Optical and BSE images of zircons grains have been supplied in Online Resource (1) Data reduction was performed with the SHRIMPTOOLS software (available from http://www.ugr.es/fbea). Associated errors are one sigma level. SHRIMP results have been provide in Online resource (2) The common lead uncorrected $^{206}Pb/^{238}U$ ages (in Ma) were plotted as a combination of Kernel Density Estimates (KDE) and histograms performed with DensityPlotter version 8.0 (Vermeesch 2012). Application of the optimal bandwidth calculated by DensityPlotter resulted in a over smoothing of the KDE in various samples. Accordingly, a common bandwidth of 40 Ma was selected for all samples. Statistically significant age populations were identified with the mixture modeling option implemented in DensityPlotter. Populations were reasonably well identified. However, in some few cases peaks of the mixture modeling do not fit the modes showed in KDE. One inadvisable procedure to fit them is to diminish the KDE bandwidth to identify various modes on the same diagram. However, a bandwidth value too low can lead to identification of spurious and non-informative modes. Bin width for histograms was set to 100 Ma. Concordia plots in Online resource 3 were done with Isoplot version 4.15 (Ludwig 2008).

Description and localization of schist samples

It has been studied eight samples taken in three areas of the Nevado–Filábride complex: the Peñones de San Francisco area (samples SF-1 and SF-2) and La Ragua area (samples RA-1, RA-2 and RA-3), which are both located in Sierra Nevada; and the Velefique area (samples VE-1, VE-2, and VE-3) in Sierra de los Filabres (Fig. 1). Samples SF-1, RA-1, RA-2, VE-1, and VE-2, were taken in the Crystalline of Sierra Nevada (Veleta unit), and SF-2, RA-3 and VE-3 in the Mischungszone (Mulhacén unit). Their stratigraphic relative positions are shown in the schematic lithological succession in Fig. 1b. It is necessary to emphasize that VE-1 and RA-1 correspond to the lower visible points of the lithological sequence, respectively, in the Sierra de los Filabres and Sierra Nevada. The rest of the samples were taken progressively in higher positions of the lithological succession. The sample SF-2 was taken in the highest structural position of the Nevado–Filábride complex succession studied in this work.

The studied samples are dark-gray schists, with the exception of VE-3 being a fine-grained bluish-schist. The major mineral phases are quartz, phengite, paragonite, and chlorite. Chloritoid has been found only in samples SF-1, RA-1; garnet in samples SF-2, RA-2, RA-3; and epidote in samples SF-2, RA-2, RA-1. Graphite, biotite, apatite, ilmenite, rutile, xenotime, and zircon appear as minor phases. Zircon grains were observed both in the matrix and as inclusions in other minerals such as garnet, albite, phengite, and paragonite.

Zircon morphology and inclusions

Zircon morphology

In the Peñones de San Francisco area, zircons are anhedral or subhedral, but a few cases of euhedral grains have been preserved. The grain size differs in the samples: SF-1 exhibits sizes between 60 and 200 µm, and in SF-2 between 40 and 120 µm. Some green-colored grains occur in sample SF-1 but generally the grains appear to be colorless, and transparent or translucent.

The zircons studied in La Ragua area sampling are anhedral. In all samples, the grain size is between 60 and 200 µm. In general, they are translucent or transparent and colorless. Nevertheless few green-, pink-, blue- and brown-colored grains can be found.

The zircons in the Velefique area sampling are anhedral or subhedral. Rounded edges are common, and elongated grains are present in zircons from sample VE-2. The size of zircon grains varies between 10 and 180 µm, but a few larger grains appear in sample VE-1 with sizes up to 300 µm. Grains are mainly colorless, and transparent or translucent, although some opaque grains are also observed in sample VE-2.

Only inherited zircons can be used for determining the MDA. Zircon grains identified as igneous in origin necessarily imply that they were inherited in the Nevado–Filábride schists. Alike, metamorphic grains formed before the deposition can be used. Conversely, as it was pointed in the introduction, metamorphic zircons formed after the deposition of sediments should be discarded. CL images of zircon grain studied in this work have proved to be a useful tool to determine the possible former origin based on zoning (Belousova et al. 2006; Corfu et al. 2003; Rubatto and Scambelluri 2003; Wu and Zheng 2004). Besides, the rounded edges observed in most of zircon grains point to a final episode of sedimentary transport and can be considered inherited regardless of their former origin (Gärtner et al. 2013).

The most common texture observed in the core and rim has been an oscillatory zone (in some cases slightly blurred) (Figs. 2, 3), which usually supports an igneous origin (Corfu et al. 2003). Some grains show blurred oscillatory zone and non-oscillatory patches which can be common features formed during a partial metamorphic recrystallization process (Corfu et al. 2003; Hoskin and Schaltegger 2003). Finally, in a few cases the observed oscillatory zone can

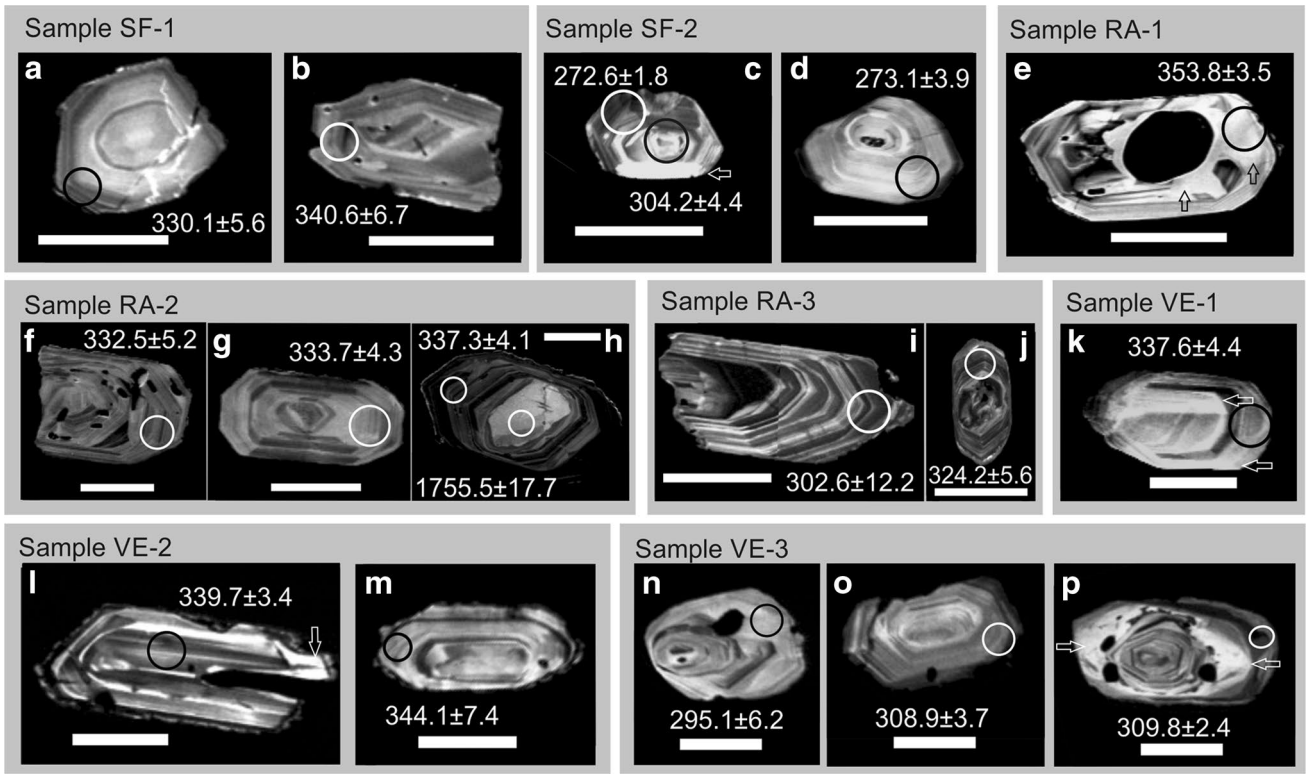

Fig. 2 Selection of cathodoluminescence images of zircons showing representative Permian and Carboniferous analyses. See text for a detailed description. Circles correspond to SHRIMP analysis points and ages are in million years. Arrows show no-zoned patches. Scale bars correspond to 50 µm

be slightly deformed, leading to convolute zoning (cores in Fig. 2 f, j).

Few zircons show a xenocrystic core surrounded by variably well-preserved oscillatory zoned rims (Figs. 2n, 3k–o). In some cases the rim preserves radial fractures formed by the expansion of a richer U core due to metamictization process (Fig. 3l) (Corfu et al. 2003; Ewing et al. 2003). However, in other examples the zircon preserves a richer U rim, and a rim which does not fracture (Fig. 3k). The origin of xenocrystic cores cannot always be deduced, but sometimes the cores show abrasion on their edges (Fig. 3k). In these cases, xenocrystic cores record a detrital episode after its formation, followed by the new rim growth.

Some grains can be recognized as metamorphic zircons based on features pointing to this origin (e.g., Wu and Zheng 2004; Rubatto 2002, 2017). These characteristics include anhedral morphology of the zircon grain and features in the CL images as: weak zoning (Fig. 3m), the presence of no-zoned patches (arrows in Figs. 2c, e, k, l, p, 3a, g, h, i, j, k, l, m, n, p), and fir-tree zoned areas (Fig. 3d). Additionally, it has been found zircons yielding Th/U < 0.1, these being commonly attributed to metamorphic zircons (Rubatto et al. 2001), even if examples of metamorphic zircons with Th/U > 0.1 have also been documented (see Rubatto 2017 and references herein). Metamorphic zircons crystallized after the deposition of the clastic sediments of the Nevado–Filábride complex are consequently not inherited, and cannot be used to determine the MDA. As it was pointed in the "Geological setting", the polyphased Alpine metamorphism which affected the Nevado–Filábride complex occurred during the Oligocene and/or Miocene, and the existence of metamorphic grains showing these age values has been taken in to account. Cenozoic age values have not been found in the present work, so the existence of metamorphic grains formed in this event can be discarded. Additionally, thin external no-luminescent rims (Figs. 2e, l, m, o, 3a, b, e, f, l, m, n) possibly were formed during Alpine metamorphism and were ignored in the SHIRMP study.

Finally, no-luminescent spots (Figs. 2b, e, f, j, l, m, n, o, p, 3f, g, h, j) have been attributed to inclusions (see below).

Description of zircon inclusions

Backscattered images combined with EDX analyses allowed to determine the morphology, size, and composition of the inclusions. In sample SF-1, there are quartz inclusions with a size ≤ 20 µm in diameter, (Fig. 4a), apatite ≤ 25 µm (Fig. 4a and insets), and xenotime ≤ 30

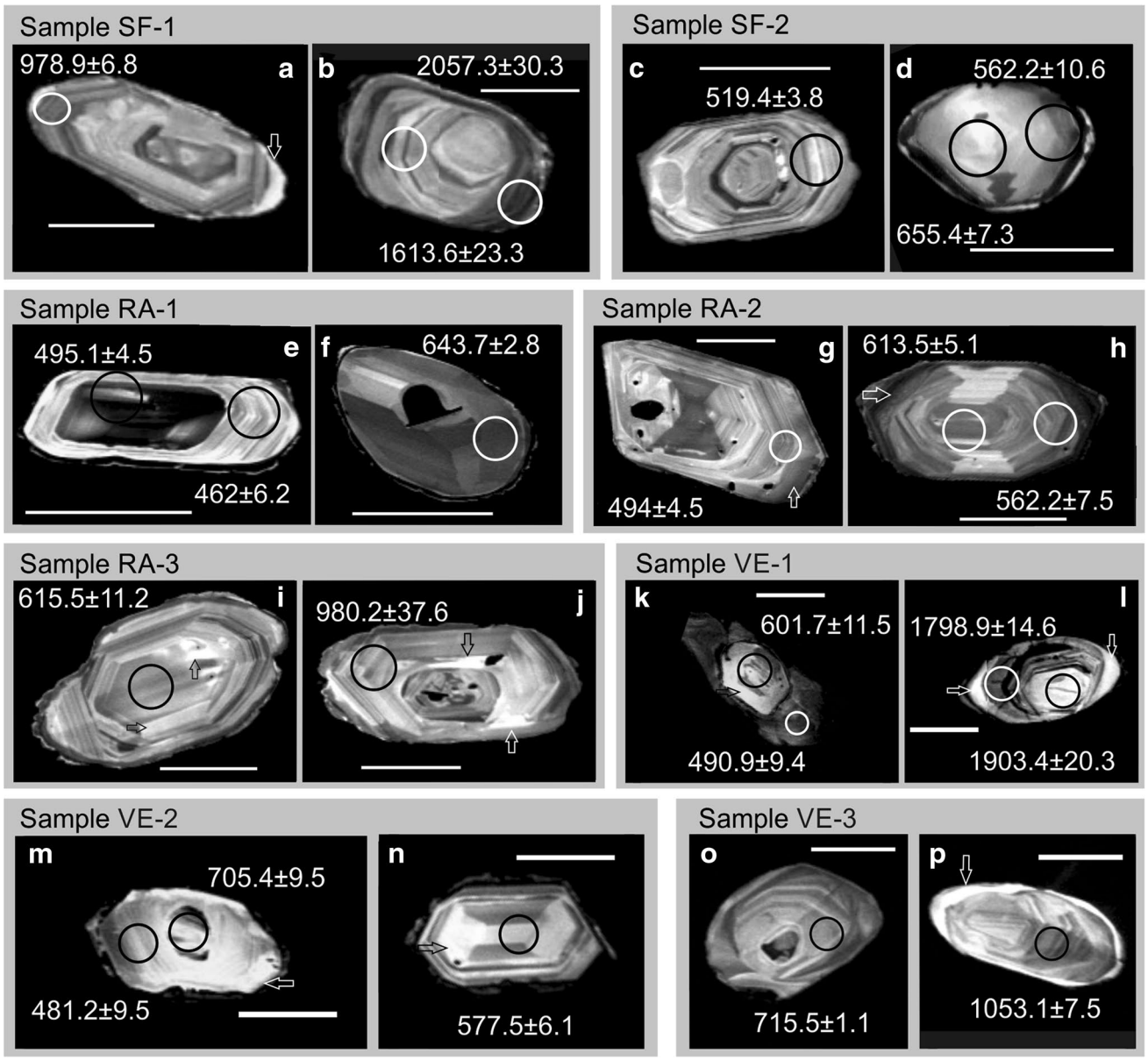

Fig. 3 Selection of cathodoluminescence images of zircons showing representative older than Carboniferous analyses. See text for a detailed description. Circles correspond to SHRIMP analysis points and ages are in million years. Arrows show no-zoned patches. Scale bars correspond to 50 μm

μm (Fig. 4b and inset). Sample SF-2 zircons show inclusions of quartz with a size ≤ 15 μm in diameter (Fig. 4c), phengite ≤ 30 μm (Fig. 4c inset), paragonite ≤ 30 μm, apatite ≤ 12 μm, albite ≤ 10 μm, and xenotime ≤ 10 μm. In the zircon grains of sample RA-1, quartz inclusions with a size ≤ 45 μm in diameter (Fig. 4d, e) were common (particularly in the youngest age zircon populations) and, to a lesser extent, chlorite ≤ 7 μm (Fig. 4e). Zircons in sample RA-2 have inclusions of quartz with a size ≤ 40 μm in diameter, phengite ≤ 6 μm (Fig. 4f), apatite ≤ 25 μm (Fig. 4f and inset; Fig. 4g), and monazite ≤ 30 μm (Fig. 4g and inset). In sample RA-3, quartz inclusions with a size ≤ 10 μm in diameter, apatite ≤ 20 μm and paragonite ≤ 4 μm were found (Fig. 4h). The main inclusions present in zircon grains from sample VE-1 are usually quartz (5–10 μm) (Fig. 4j) and apatite inclusions (4 μm) (Fig. 4i, j). Rutile inclusions ≤ 5 μm are less common (Fig. 4i). Sample VE-2 zircons exhibits quartz as main inclusion, showing a wide variability of sizes. In general, quartz inclusions were small, ≤ 7 μm in diameter (Fig. 4k, l), but a few other ones were significantly larger (e.g., 75 μm in the zircon grain shown in Fig. 4m). Apatite (≤ 8

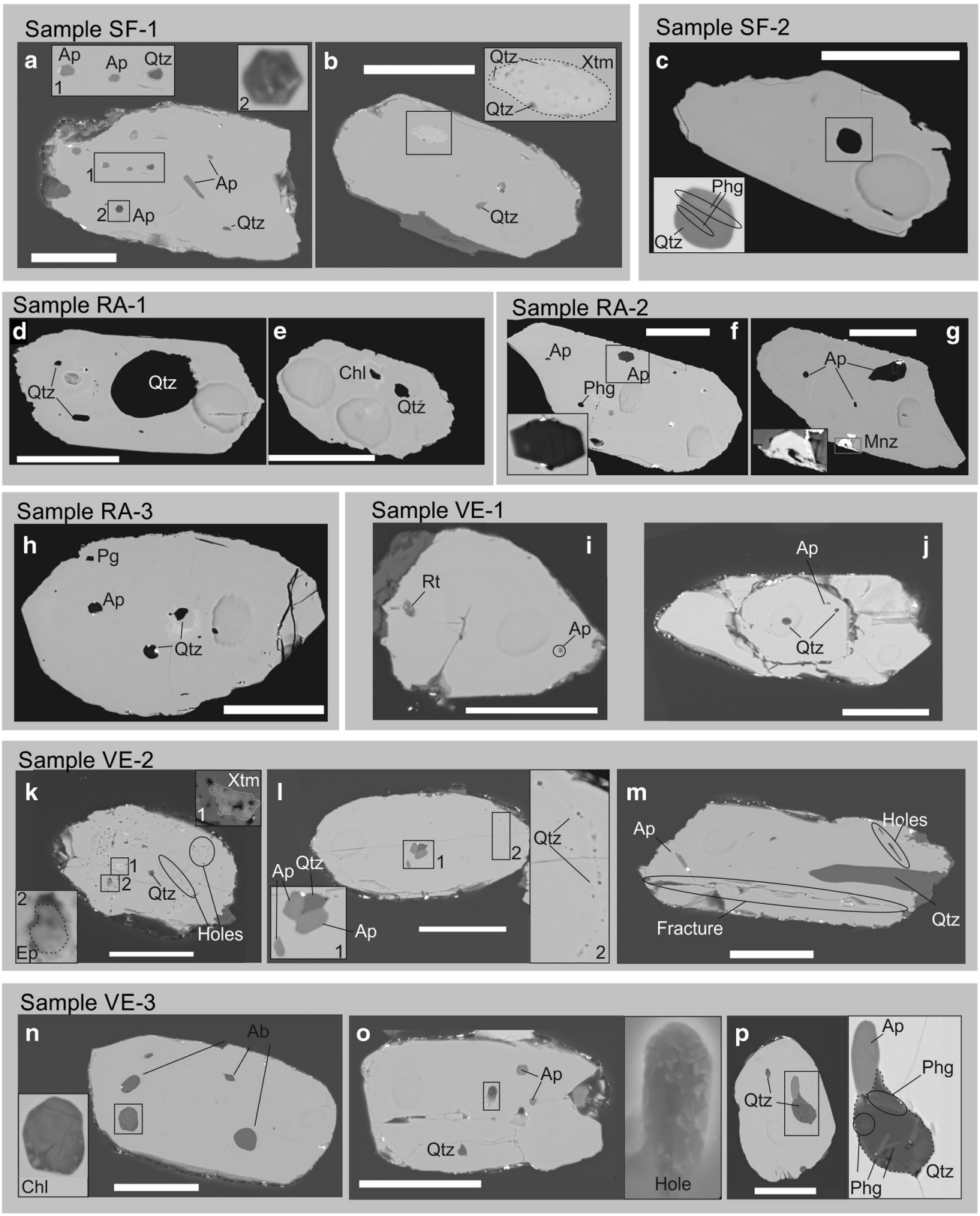

Fig. 4 Selection of BSE images of the zircons and of the most significant inclusions observed. *Qtz* Quartz, *Phg* phengite, *Ap* apatite, *Xtm* xenotime, *Chl* chlorite, *Mnz* monazite, *Pg* paragonite, *Rt* rutile, *Ep* epidote, *Ab* albite. Scale bars correspond to 50 µm

μm) (Fig. 4l, m), xenotime (5 μm) (Fig. 4k and inset 1) and epidote (5 μm) (Fig. 4k and inset 2) inclusions were also found. In sample VE-3, the inclusions are quartz ≤ 25 μm (Fig. 4o, p), apatite ≤ 15 μm (Fig. 4o, p), chlorite ≤ 20 μm (Fig. 4n and inset), albite ≤ 15 μm (Fig. 4n) and phengite of 5 μm (Fig. 4p and inset). The zircons studied in the eight samples exhibit holes, attributed to fluid inclusions, or fractures on the surface (e.g., Fig. 4k, m, o). Some of these holes have been filled by gold coating in the images.

Geochronology results

Below it is summarize the $^{206}Pb/^{238}U$ zircon age provided by the analyses for each sample and grouped by age populations. The distribution histogram and the KDE plots are shown in Fig. 5 for the Mischungszone (Mulhacén unit) samples (SF-2, RA-3 and VE-3), and Fig. 6 for the Crystalline of Sierra Nevada (Veleta unit) samples (SF-1, RA-1, RA-2, VE-1 and VE-2). Age populations obtained after mixture modeling are detailed for each sample. Online Resource 2 and Online Resource 3, correspond to the SHRIMP results, and the Wetherill plots, respectively.

The majority of the analyses were acquired on the outermost rim of each zircon grain (excluding the last Alpine metamorphic event). Nevertheless, some zircon grains were analyzed twice for core and rim. In most cases, the ages obtained for these two domains are different, but sometimes core and rim analyses yield the same age within error. Zircon grains that may have lost lead, according to the high U concentration observed (> 3000 ppm) were, therefore, rejected from the analyses. Analyses with a discordance value > 10% were discarded. The results are described first for the Mischungszone (Mulhacén unit) samples, followed by the Crystalline of Sierra Nevada (Veleta unit) samples.

Mischungszone (Mulhacén unit) $^{206}Pb/^{238}U$ age populations

Sample SF-2 $^{206}Pb/^{238}U$ age populations

In sample SF-2, 52 zircon analyses (39 in rims and 13 in cores) were obtained; six of them were rejected because of their high discordance (> 10%). The youngest analysis is 232 ± 1 Ma. In this sample, analyses defined an age population at 269.6 ± 0.9 Ma, followed by a prominent age population at 601.2 ± 0.9 Ma (Fig. 5).

Sample RA-3 $^{206}Pb/^{238}U$ age populations

In sample RA-3, 54 analyses (38 in rims and 16 in cores) were obtained; four of them were rejected because of their high discordance (> 10%). The youngest analysis

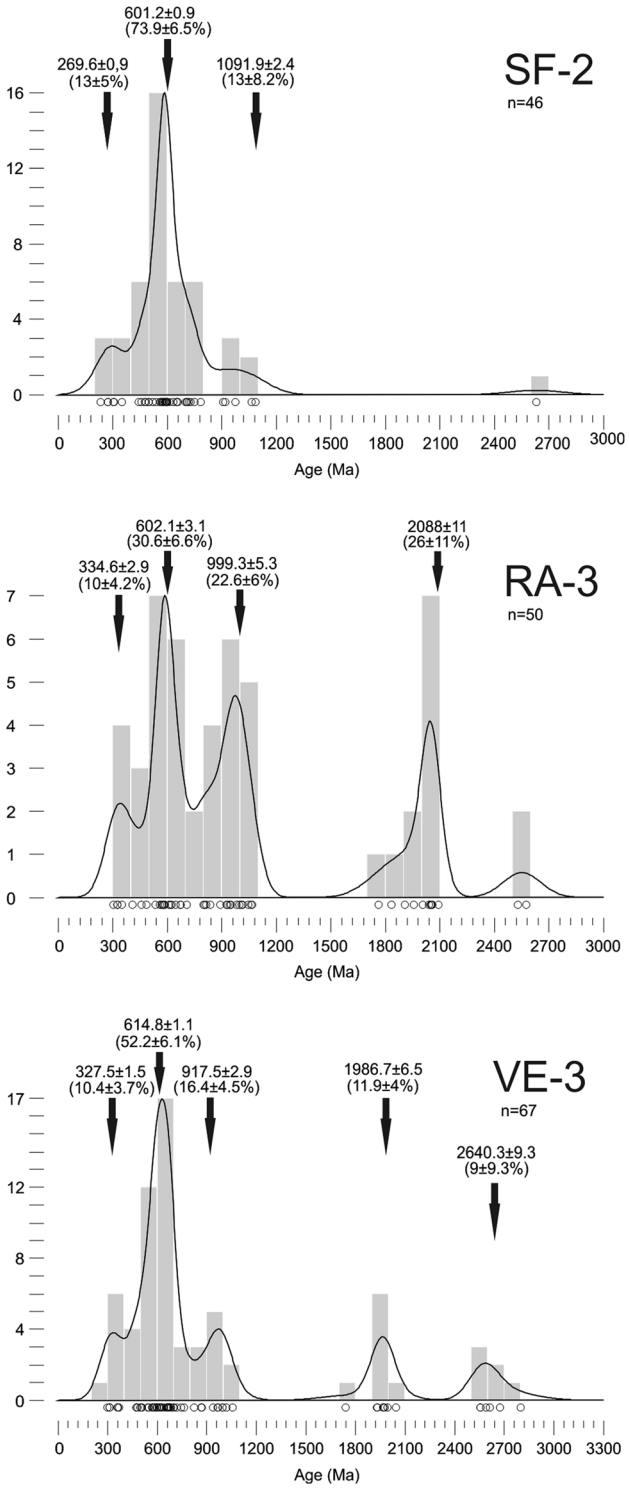

Fig. 5 Distribution histogram (grey bars) and kernel density estimates (black lines) showing the $^{206}Pb/^{238}U$ zircon ages obtained from the Mischungszone (Mulhacén unit) samples (SF-2, RA-3, VE-3). Arrows mark the age populations after mixture modeling. Circles in the lower part of each diagram represent single analyses. Diagrams have been calculated with DensityPlotter version 8.0 (Vermeesch 2012) using lead uncorrected $^{206}Pb/^{238}U$ ages and one sigma level errors. Analyses with discordance > 10% were discarded. Selected analyses are included in Online resource 2

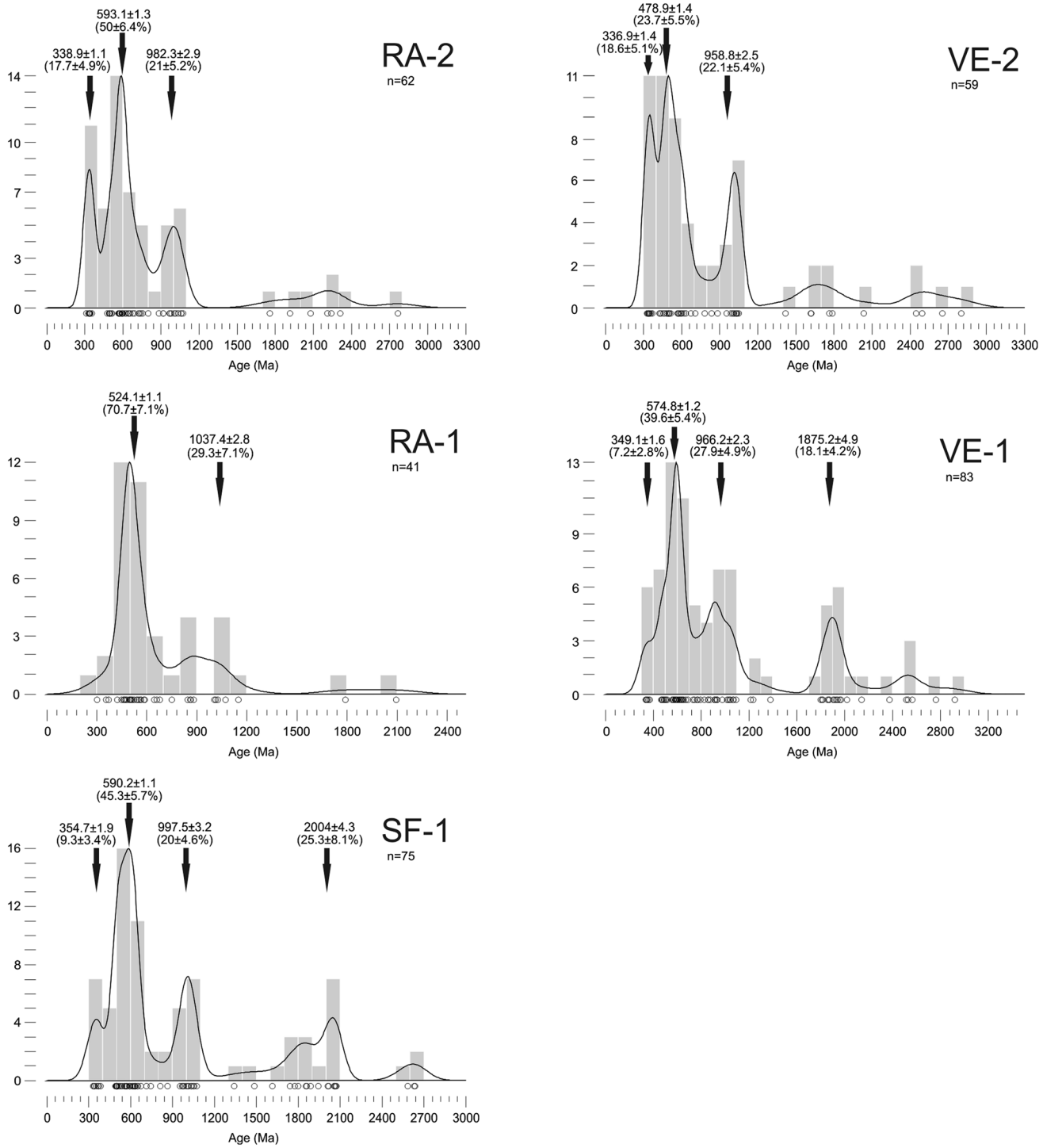

Fig. 6 Distribution histogram (grey bars) and kernel density estimates (black lines) showing the $^{206}Pb/^{238}U$ zircon ages obtained from the Crystalline of Sierra Nevada (Veleta unit) samples (SF-1, RA-2, RA-1, VE-2, VE-1). Arrows mark the age populations after mixture modeling. Circles in the lower part of each diagram represent single analyses. Diagrams have been calculated with DensityPlotter version 8.0 (Vermeesch 2012) using lead uncorrected $^{206}Pb/^{238}U$ ages and one sigma level errors. Analyses with discordance > 10% were discarded. Selected analyses are included in Online resource 2

is 303 ± 12 Ma. A younger age population is observed at 334.6 ± 2.9 Ma, followed by two prominent probability peaks at 602.1 ± 3.1 and 999.3 ± 5.3 Ma. Finally there is a remarkable Paleoproterozoic population at 2088 ± 11 Ma (Fig. 5).

Sample VE-3 $^{206}Pb/^{238}U$ age populations

In sample VE-3, 70 analyses (63 in rims and 7 in cores) were obtained; three of them were rejected because of their high discordance (> 10%). The youngest analysis is 295 ± 6 Ma. The youngest age population is 327.5 ± 1.5 Ma. The biggest age population is 614.8 ± 1.1 Ma, and is followed by small populations at 917.5 ± 2.9, 1986.7 ± 6.5 and 2640.3 ± 9.3 Ma (Fig. 5).

Crystalline of Sierra Nevada (Veleta unit) $^{206}Pb/^{238}U$ age populations

Sample SF-1 $^{206}Pb/^{238}U$ age populations

In sample SF-1, 78 analyses (70 in rims and 8 in cores) were obtained; three of them were rejected because of their high discordance (> 10%). The youngest analysis, 330 ± 6, Ma, is included in an age population of 354.7 ± 1.9 Ma. Two prominent probability peaks are present at 590.2 ± 1.1 and 997.5 ± 3.2 Ma. Finally several Paleoproterozoic analyses define an age population at 2004 ± 4.3 Ma (Fig. 6).

Sample RA-1 $^{206}Pb/^{238}U$ age populations

In sample RA-1, 48 analyses (34 in rims and 14 in core) were obtained; seven of them were rejected because their high discordance (> 10%). The youngest analysis is 300 ± 4 Ma. The youngest statistical significant population yield an age of 524.1 ± 1.1 Ma, followed by scattered Neoproterozoic and Mesoproterozoic analyses (Fig. 6).

Sample RA-2 $^{206}Pb/^{238}U$ age populations

In sample RA-2, 64 analyses (49 in rims and 15 in cores) were obtained; two of them were rejected because of their high discordance (> 10%). The youngest analysis, 309 ± 6 Ma, is included in a population at 338.9 ± 1.1 Ma. The most prominent probability peak is 593.1 ± 1.3 Ma, and is followed a smaller population at 982.3 ± 2.9 Ma. Finally, a minor amount of analyses show Paleoproterozoic ages (Fig. 6).

Sample VE-1 $^{206}Pb/^{238}U$ age populations

In sample VE-1 86 analyses (77 in rims and 9 in cores) were obtained; three of them have been rejected because of their high discordance (> 10%). The youngest analysis is 335 ± 6 Ma. The youngest age population is present at 349.1 ± 1.6 Ma. The most prominent probability peak is 574.8 ± 1.2 Ma. A broad population is present at 966.2 ± 2.3, and 1875.2 ± 4.9 Ma, Finally there is some representation of Archaean ages (Fig. 6).

Sample VE-2 $^{206}Pb/^{238}U$ age populations

In sample VE-2, 70 analyses (58 in rims and 12 in cores) were obtained; eleven of them were rejected because of their high discordance (> 10%). The youngest analysis, 326 ± 4 Ma, is included in an age population of 336.9 ± 1.4 Ma, closely followed by a probability peak at 478.9 ± 1.4 Ma. A smaller age population is found at 958.8 ± 2.5 Ma (Fig. 6).

Discussion

Age of the metasediments

The youngest age populations that are statistically significant (formed by number of analyses ≥ 3) for each sample are shown in Table 1. The youngest age populations identified in the lowermost sample in each unit can be used to estimate MDAs.

In the Crystalline of Sierra Nevada (Veleta unit) four of the five samples (SF-1, RA-2, VE-1 and VE-2) show Carboniferous youngest age populations (Table 1). In particular, the sample VE-1 which was taken in the lowest part of the Crystalline of Sierra Nevada (Veleta unit) (Fig. 1b), shows a youngest age population of 349.1 ± 1.6 Ma. This age can be assumed as the most probable MDA of the unit.

In the Mischungszone (Mulhacén unit) two of the three samples show Carboniferous youngest age populations (RA-3 and VE-3) (Table 1). In this unit, sample RA-3 was taken in the lowermost position (Fig. 1b) and the youngest

Table 1 Youngest statistically significant age populations obtained in the studied samples

Sample	Youngest age population (Ma)	Unit
SF-2	269.6 ± 0.9	Mischungzone (Mulhacén unit)
RA-3	334.6 ± 2.9	
VE-3	327.5 ± 1.5	
SF-1	354.7 ± 1.9	Crystalline of Sierra Nevada (Veleta unit)
RA-2	338.9 ± 1.1	
RA-1	524.1 ± 1.1	
VE-2	336.9 ± 1.4	
VE-1	349.1 ± 1.6	

age population in this sample is 334.6 ± 2.9 Ma, and corresponds to the most probable MDA of this unit.

In samples SF-2 and RA-1 the number of Carboniferous analyses is insufficient ($n < 3$) to define statistically representative age populations. Nevertheless, a Carboniferous participation is still present in these two samples (Figs. 5, 6), and are in line with the previous Carboniferous estimations.

Comparison with previous results and geological implications

The youngest age populations in the Mischungszone (Mulhacén unit) (Table. 1), have been compared with the ages determined for this unit in previous works. Various studies have been oriented to dating of zircons included in orthogneisses. Age estimations comprise: Martínez-Martínez et al. (2010), of 304 ± 23 and 314 ± 7 Ma, and Gómez-Pugnaire et al. (2004) of 301 ± 7 Ma, in the western part of Sierra Nevada; and those of Gómez-Pugnaire et al. (2012), of 282 ± 5 to 295 ± 3 Ma, and Ruiz-Cruz and Sanz de Galdeano (2017) of ~ 286 Ma, in the south-western area of Sierra Nevada. Youngest age populations in samples RA-3 and VE-3 are older than the cited. The differences between our results and literature can be attributed to the different origin of the zircons: detrital zircons are inherited in the sediment, while zircons obtained from the orthogneisses yield ages later the deposition. Only youngest age population in sample SF-2 is younger than the ages reported by those authors. Bashkirian (315 ± 2–323 ± 2 Ma) conodonts found by Rodríguez et al. (2017) point to an age younger than our results in samples RA-3 and VE-3, which, according to our interpretation, shares the stratigraphic position with these authors' samples. Again, differences are not incompatible because detrital zircons can be older than the fauna included in the sediment. On the contrary, sample SF-2 was taken in an upper part the lithological succession, where it can be expected younger sediments.

The lack in the literature of radiometric ages of the sediment protolith in the Crystalline of Sierra Nevada (Veleta unit) prevents to compare the ages obtained in samples SF-1, RA-1, RA-2, VE-1 and VE-2, with any other absolute age estimation. Until our knowledge, the only no-radiometric estimations for this unit were yielded from pre-Cambrian (Gomez-Pugnaire et al. 1982) and Devonian (Laborda-López et al. 2015; Lafuste and Pavillon 1976) fossils (these latter not in the Sierras Nevada and Filabres, but eastwards in the complex), older than our results in samples SF-1, RA-2, VE-1 and VE-2, and in any case similar to sample RA-1 youngest age population.

The predominance, in this work, of Carboniferous youngest age populations does not necessary implies that the totality of the sediment protolith was deposited during this period. According to the results a younger age of the sediment protolith cannot be excluded. Gómez-Pugnaire et al. (2012) age estimations in orthogneisses from the upper part of the complex (see their sample CB-4) allow obtaining minimum ages of deposition of 282 ± 5 Ma for the schists in the Mischungszone (Mulhacén unit). Therefore, combining the minimum age with the MDAs obtained in the present work it is possible to narrow the time lapse of deposition of the Nevado–Filábride sediments, comprising the Crystalline of Sierra Nevada (Veleta unit) and the Mischungszone (Mulhacén unit). As the youngest age population obtained in the lowest sample studied (VE-1) is 349.1 ± 1.6 Ma, the deposition of these sediments should happen between ca. 282–349 Ma. This period could be shorter because the rock can be younger than the estimated MDA. The present thickness existing between the stratigraphic positions of the samples from Gomez-Pugnaire et al. (2012) and the sample VE-1 is ~ 4000 to 5000 m, according to our estimations. As the sequence could present several tectonic repetitions, the actual estimation of the deposited sediment volume, even if it can be high, cannot be estimated in this work.

Interpretation of older age populations and similarity between units

In addition to the Carboniferous age populations, other common age populations have been found in the studied zircons. All the samples show a clear domain ranging ca. 490–630 Ma, pointing to a Cadomian growth of many of these zircons. Moreover, all samples, and to a lesser extent in sample SF-2, exhibit age populations ca. 910–1010 Ma (possibly Grenville). Paleoproterozoic ages are particularly present in samples SF-1, RA-3, VE-1, but absent in sample SF-2 and almost absent in sample RA-1. Those two samples reported few analyses > 1200 Ma insufficient to define age populations. Finally, although there is a representation of Archaean analyses in all samples, it is remarkable only in sample VE-3.

The similarity between various population ages in samples attributed to the Crystalline of Sierra Nevada (Veleta unit) (samples SF-1, RA-1, RA-2, VE-1 and VE-2), and the Mischungszone (Mulhacén unit) (samples SF-2, RA-3 and VE-3,) implies a common source area for the detrital zircons. Even when both units share the same detrital inheritance pattern, do not imply that both units constitute a continuous sequence. Therefore, the observed similarity is not conclusive in relation to the proposed division of the Nevado–Filábride complex into several tectonically superposed units. Nevertheless, the youngest age populations in the upper samples of the complex (additionally confirmed by dating in orthogneisses) are younger than those of the lower samples. This finding does not necessarily support the proposed tectonic differentiation of the Nevado–Filábride complex. On the contrary, the observed tendency can be

interpreted as a result of a continuity in the sequence where the Crystalline of Sierra Nevada (Veleta unit) is the older part of the complex, and the Mischungszone (Mulhacén unit), on the top, is the younger part.

Origin of inclusions

The study of SEM images and EDX patterns, combined with the CL images, allowed constrain former origin of the inclusions and their relationship with the host zircon. Initial approach focused on the determination of the primary or secondary origin of the inclusions. Primary inclusions can be present in both igneous zircons and metamorphic regrowth. In the first case, the CL image shows a mostly unaltered oscillatory pattern and no-alterations around the inclusion. The common interpretation is that the inclusion was trapped during the growth of the zircon. Otherwise, inclusions can be found in metamorphic regrowth, recrystallizations, or in metamorphic rims surrounding xenocrystic igneous cores. In those cases the oscillatory pattern can be absent, and inclusions are related to no-zoned patches, weak zoning, etc. Finally, inclusions related to fractures can be interpreted as secondary inclusions formed after precipitation from fluids. Therefore, CL images show patched zoning and/or disturbed structures formed after the zircon-secondary inclusion interaction (Wu and Zheng 2004).

Primary inclusions

Most of the primary inclusions reported in this paper are inclusions trapped in oscillatory zoned zircons interpreted as igneous in origin. Quartz (Fig. 2i, o) and apatite (Fig. 4f, g, o) are the main primary inclusions. Phengite (Fig. 4c, f), monazite and xenotime (which in some cases is included by small quartz grains, see Fig. 4b) are occasional. Apatite, monazite and xenotime are not always present in the sample matrix. Therefore, their inclusion in zircons during the igneous phase seems plausible. Quartz, apatite and phengite occupy positions in cores and rims, while xenotime and monazite usually are found in mantle and rim. Some quartz and apatite are present in cores showing oscillatory pattern partially fainted. In those cases an igneous origin has been attributed to inclusions and cores, later affected by a metamorphic event which led to alteration of the oscillatory pattern. In general, igneous primary inclusions have been found in zircons which yield SHRIMP analyses of ca. 300–380 Ma. Only few inclusions of quartz, apatite and xenotime are included in zircons showing analyses ca. 520 Ma, and a quartz inclusion have been found in a rim showing analyses of ca. 620 Ma.

Zircons showing metamorphic regrowth are occasionally included by metamorphic minerals as paragonite (Fig. 4h), albite (Fig. 4n) and chlorite (Fig. 4n). The regrowth envelop oscillatory zoned cores, commonly fainted and included by quartz and apatite (Fig. 4j). SHRIMP analyses in the regrowth yield dates ranging ca. 310–350 Ma, interpreted as the age when paragonite, plagioclase and chlorite were formed during metamorphism. The igneous cores show analyses ~ 350, ~ 600 and ~ 1000 Ma, which point to the age of previous igneous phases. Results support the complex zircon growth story which includes several crystallization steps under different conditions. Conversely, zircon in Fig. 4e shown an obliterated oscillatory zoned core included by quartz and chlorite, surrounded by an oscillatory rim. In this case, an even more complex story can be inferred, including an initial igneous event followed by possible alteration during metamorphism and, finally, new growth under igneous conditions.

Secondary inclusions

Inclusions related with fractures are quartz (Fig. 4d, l and insets, and 4m), apatite (Fig. 4l and insets, 4m and 4o), phengite (in some cases included in quartz, see Fig. 4p), paragonite, rutile (Fig. 4i), monazite (Fig. 4g), xenotime and epidote (Fig. 4k and insets). Samples which contain those inclusions additionally show them as phases in the matrix. We interpret that precipitation of inclusions occurred during the Alpine metamorphism (see the Geological setting).

Conclusions

Detrital zircons were dated to obtain in situ SHRIMP U–Pb ages in eight mica-schist samples from the Nevado–Filábride complex. The most notable findings in this study are:

The youngest age populations obtained in the Crystalline of Sierra Nevada (approximately equivalent to the Veleta unit) in four of the five samples are Carboniferous. Lower sample youngest age population, 349.1 ± 1.6 Ma, is the statistically estimation of the maximum deposition age of this unit.

The youngest age populations obtained in two of the three samples in the Mischungszone (approximately equivalent to the Mulhacén unit) are Carboniferous. The sample taken in the upper part of the unit shows a Permian youngest age population (269.6 ± 0.9 Ma). The lower sample youngest age population, 334.6 ± 2.9 Ma, is the statistically estimation of the maximum deposition age of this unit.

Age results obtained in the Mischungszone (Mulhacén unit) are in agreement with previous estimations of the minimum age for the sedimentation.

Combining the estimated MDA obtained in the lowermost sample (VE-1) with the minimum age of deposition obtained by Gómez-Pugnaire et al. (2012) allow constraining the

deposition of the Nevado-Filábride complex sediments in a maximum period of 67 Ma (between ca. 282 and 349 Ma).

In the studied samples, common age clusters have been found at ca. 490–630 and ca. 910–1010 Ma.

The similarities between the age populations found in the Crystalline of Sierra Nevada (Veleta unit) and the Mischungszone (Mulhacén unit) samples suggest a common source area for the sediments. Results show progression from older age populations in samples from the Crystalline of Sierra Nevada (Veleta unit) to younger age populations in samples from the Mischungszone (Mulhacén unit). This can be attributed to a continuity between both units, and the lack of a tectonically superposition.

Inclusions found in zircons are manly quartz and apatite, and to a lesser extent phengite, paragonite, chlorite, rutile, epidote, monazite, xenotime and albite. Inclusions in oscillatory zoned zircons have been interpreted as trapped during zircon growth in igneous episodes ca. 300–380, 520 and 620 Ma. Paragonite, albite and chlorite inclusions have been found in no-zoned and weak-zoned patches interpreted as formed during metamorphic regrowth ranging ca. 310–350 Ma.

Acknowledgements The authors thank Urs Klötzli and Jesús Galindo, whose inestimable reviews have been of great help to improve the work. They would also like to express our gratitude to María Dolores Ruiz Cruz for the revision of the manuscript; Pierre Lanari (Institute of Geological Sciences, University of Bern) and Irene Pérez (Facultad de Ciencias, Universidad de Granada) for their useful comments on the manuscript; Pilar Montero and Fernando Bea (Facultad de Ciencias, Universidad de Granada) for gathering and processing the SHRIMP data; Isabel Nieto for extracting and separating the zircons; and Isabel Sánchez of CIC (Facultad de Ciencias, Universidad de Granada) for her help in gathering the SEM data. This study was supported by the Ministerio de Economía y Competitividad (Spain) (Project CGL 2012–31872), and by the project DAMAGE (AEI/FEDER CGL2016-80687-R). This is the IBERSIMS contribution number 53.

References

Andersen T (2005) Detrital zircons as tracers of sedimentary provenance: limiting conditions from statistics and numerical simulation. Chem Geol 216:3–4, 249–270

Andriessen PAM, Hebeda EH, Simon OJ, Verschure RH (1991) Tourmaline K–Ar ages compared to other radiometric dating systems in Alpine anatectic leucosomes and metamorphic rocks (Cyclades and Southern Spain). Chem Geol 91:33–48

Augier R, Booth-Rea G, Agard P, Martínez-Martínez JM, Jolivet L, Azañón JM (2005) Exhumation constraints for the lower Nevado–Filabride Complex (Betic Cordillera, SE Spain): a Raman thermometry and Tweequ multiequilibrium thermobarometry approach. B Soc Geol Fr 176(5):403–416

Behr WM, Platt JP (2012) Kinematic and thermal evolution during two-stage exhumation of a Mediterranean subduction complex. Tectonics 31:4

Belousova EA, Griffin WL, O´Reilly SY (2006) Zircon crystal morphology, trace element signatures and Hf isotope composition as a tool for petrogenetic modelling: examples from Eastern Australian Granitoids. J Petrol 47:329–353

Booth-Rea G, Martínez-Martínez JM, Giaconia F (2015) Continental subduction, intracrustal shortening and coeval upper-crustal extension: P-T evolution of subducted south-Iberian paleomargin metapelites (Betics, SE Spain). Tectonophysics 663:122–139

Brouwer HA (1926) Zur Tektonik der betischen Kordilleren. Geol Rundsch 17:332–336

Corfu F, Hanchar JM, Hoskin PWO, Kinny P (2003) Atlas of zircon textures. In: Hanchar JM, Hoskin PWO (eds) Zircon. Rev Mineral Geochem, vol 53. Mineralogical Society of America, Washington DC, pp 469–500

Davis DW, Williams IS, Krogh TE (2003) Historical development of U–Pb geochronology. In: Hanchar JM, Hoskin PWO (eds) Zircon. Rev Mineral Geochem, vol 53. Mineralogical Society of America, Washington DC, pp 145–181

de Jong K (1991) Tectonometamorphic studies and radiometric dating in the Betic Cordilleras (SE Spain) - with implications for the dynamics of extension and compression in the western Mediterranean area. Thesis Vrije Universiteit Amsterdam, p 204

de Jong K (1993) The tectonometamorphic evolution of the Veleta Complex and the development of the contact with the Mulhacén Complex (Betic Zone, SE Spain). Geol Mijnbouw 71:227–237

de Jong K, Bakker H (1991) The Mulhacen and Alpujarride Complex in the eastern Sierra de los Filabres, SE Spain: litho-stratigraphy. Geol Mijnbouw 70:93–103

Dickinson WR, Gehrels G (2009) Use of U–Pb ages of detrital zircons to infer maximum depositional ages of strata: a test against a Colorado Plateau Mesozoic database. Earth Planet Sci Lett 288:115–125

Díez Fernández R, Martínez Catalán JR, Gerdes A, Abati J, Arenas R, Fernández-Suárez J (2010) U–Pb ages of detrital zircons from the Basal allochthonous units of NW Iberia: provenance and paleoposition on the northern margin of Gondwana during the Neoproterozoic and Paleozoic. Gondwana Res 8(2–3):385–399

Egeler CG (1963) On the tectonics of the eastern Betic Cordilleras. Geol Rundsch 53:260–269

Egeler CG, Simon OJ (1969) Orogenic evolution of the Betic zone (Betic cordilleras, Spain), with emphasis on the nappe structures. Geol Mijnbouw 48:296–305

Ewing R, Meldrum A, Wang L, Weber W, Corrales L (2003) Radiation effects in zircon. Rev Mineral Geochem 53:387–425

Fallot P (1948) Les Cordillères bétiques. Estud Geol 4:83–173

Fedo CM, Sircombe KN, Rainbird RH (2003) Detrital zircon analysis of the sedimentary record. Rev Mineral Geochem 53:277–303

Galindo-Zaldívar J (1993) Geometría de las deformaciones neógenas en Sierra Nevada (Cordilleras Béticas). Monografía Tierras del Sur, Granada

Gärtner A, Linnemann U, Sagawe A, Hofmann M, Ullrich B, Kleber A (2013) Morphology of zircon crystal grains in sediments-characteristics, classifications, definitions. J Central Eur Geol 59:65–73

Gehrels G (2012) Detrital zircon U–Pb geochronology: current methods and new opportunities. In: Busby C, Azor A (eds) Tectonics of sedimentary basins: recent advances. Wiley-Blackwel, Chichester, pp 47–62

Gehrels G (2014) Detrital zircon U–Pb geochronology applied to tectonics. Annu Rev Earth Planet Sci 42:127–149

Gómez-Pugnaire MT, Chacón J, Mitrofanov F, Timofeev V (1982) First report on pre-Cambrian rocks in the graphite-bearing series of the Nevado–Filábride Complex (Betic Cordilleras, Spain). N Jb Geol Paliíont Mh 3:176–180

Gómez-Pugnaire MT, Braga JC, Martín JM, Sassi FP, Del Moro A (2000) Regional implications of a Palaeozoic age for the Nevado–Filabride cover of the Betic Cordillera, Spain. Schweiz Miner Petrogr Mitt 80:45–52

Gómez-Pugnaire MT, Galindo-Zaldívar J, Rubato D, González-Lodeiro F, López Sánchez-Vizcaino V, Jabaloy A (2004) A reinterpretation of the Nevado–Filábride and Alpujárride Complexes (Betic Cordillera): field, petrography and U–Pb ages from orthogneisses (western Sierra Nevada, S Spain). Schweiz Miner Petrogr Mitt 84:303–322

Gómez-Pugnaire MT, Rubatto D, Fernández-Soler JM, Jabaloy A, López-Sánchez-Vizcaíno V, González-Lodeiro F, Galindo-Zaldívar J, Padrón-Navarta JA (2012) Late Variscan magmatism in the Nevado–Filábride Complex: U–Pb geochronologic evidence for the pre-Mesozoic nature of the deepest Betic complex (SE Spain). Lithos 146–147:93–111

Hoskin PWO, Schaltegger U (2003) The composition of zircon and igneous and metamorphic petrogenesis. In: Hanchar JM, Hoskin PWO (eds) Zircon: rev mineral geochem, vol 53. Mineralogical Society of America, Washington DC, pp 27–62

Kirkland CL, Strachan RA, Prave AR (2008) Detrital zircon signature of the Moine Supergroup, Scotland: contrasts and comparisons with other Neoproterozoic successions within the circum-North Atlantic region. Precambrian Res 163:332–350

Kosler J, Sylvester PJ (2003) Present trends and the future of zircon in U–Pb geochronology: laser ablation ICPMS. In: Hanchar JM, Hoskin PWO (eds) Zircon: rev mineral geochem, vol 53. Mineralogical Society of America, Washington DC, pp 243–275

Laborda-López C, Aguirre J, Stephen K, Donovan SK, Navas-Parejo P, Rodríguez S (2015) Fossil assemblages and biostratigraphy of metamorphic rocks of Nevado–Filábride Complex from the Águilas tectonic arc (SE Spain). Span J Palaeontol 30(2):275–292

Lafuste MLJ, Pavillon MJ (1976) Mise en évidence d´Eifélien daté au sein des terrains métamorphiques des zones internes des Cordillères bétiques. Intérêt de ce nouveau repére stratigraphique. CR Acad Sci Paris 283(2):1015–1018

Litty C, Lanari P, Burn M, Schlunegger F (2017) Climate-controlled shifts in sediment provenance inferred from detrital zircon ages, Western Peruvian Andes. Geology 45:59–62

López-Sánchez-Vizcaíno V, Rubatto D, Gómez-Pugnaire MT, Trommsdorff V, Müntener O (2001) Middle Miocene high-pressure metamorphism and fast exhumation of the Nevado–Filábride Complex, SE Spain. Terra Nova 13:327–332

Ludwig K (2008) User's manual for Isoplot 3.6: a geochronological toolkit for Microsoft Excel, Berkeley Geochronology Centre. Spec Pub 4:1–71

Martínez-Martínez JM, Soto JI, Balanyá JC (2002) Orthogonal folding of extensional detachments: structure and origin of the Sierra Nevada elongated dome (Betics, SE Spain). Tectonics 21:1–22

Martínez-Martínez JM, Torres-Ruiz J, Pesquera A, Gil-Crespo PP (2010) Geological relationships and U–Pb zircon and 40 Ar/39Ar tourmaline geochronology of gneisses and tourmalinites from the Nevado–Filabride Complex (western Sierra Nevada, Spain): tectonic implications. Lithos 119:238–250

Meinhold G, Morton AC, Avigad D (2013) New insights into peri-Gondwana paleogeography and the Gondwana super-fan system from detrital zircon U–Pb ages. Gondwana Res 23(2):661–665

Monié P, Galindo-Zaldívar J, González-Lodeiro F, Goffé B, Jabaloy A (1991) $^{40}Ar/^{39}Ar$ geochronology of Alpine tectonism in the Betic Cordilleras (southern Spain). J Geol Soc Lond 148:288–297

Nieto JM (1996) Petrología y geoquímica de los ortogneises del complejo del Mulhacén, Cordilleras Béticas. Universidad de Granada, Granada

Nieto JM, Puga E, Monié P, Díaz de Federico A, Jagoutz E (1997) High-pressure metamorphism in metagranites and orthogneisses from the Mulhacén Complex (Betic Cordillera, Spain). Terra Nova 9(Supl):22–23 **(abstract 1)**

Pérez-Cáceres I, Martínez Poyatos D, Simancas JF, Azor A (2017) Testing the Avalonian affinity of the South Portuguese Zone and the Neoproterozoic evolution of SW Iberia through detrital zircon populations. Gondwana Res 42:177–192

Priem HNA, Boelrijk NAJM., Hebeda EH, Verschure RM (1966) Isotopic age determinations on tourmaline granite-gneiss and a metagranite in the Eastern Betic Cordilleras, SE Spain. Geol Mijnbouw 45:184–187

Puga E (1976) Investigaciones petrológicas en Sierra Nevada Occidental. Ph. D. Thesis, Universidad de Granada, p 279

Puga E, Díaz de Federico A, Nieto JM (2002) Tectonostratigraphic subdivision and petrological characterisation of the deepest complexes of the Betic zone: a review. Geodin Acta 15:23–43

Rodríguez R, Jabaloy A, Navas P, Martín-Algarra A (2017) Lower Bashkirian conodonts from the Nevado-Filabride complex (Betic Cordilleras, Spain): tectonic and palaeogeographic implications. Geophys Res Abstr 19:13925

Rónadh C, Coleman DS, Chokel CB, DeOreo SB, Wooden JL, Collins AS, De Waele B, Kröner A (2004) Proterozoic tectonostratigraphy and paleogeography of Central Madagascar derived from detrital zircon U–Pb age populations. J Geol 112(4):379–399

Rubatto D (2002) Zircon trace element geochemistry: partitioning with garnet and the link between U–Pb ages and metamorphism. Chem Geol 184(1–2):123–138

Rubatto D (2017) Zircon: the metamorphic mineral. Rev Mineral Geochem 83:261–295

Rubatto D, Scambelluri M (2003) U–Pb dating of magmatic zircon and metamorphic baddeleyite in the Ligurian eclogites (Voltri Massif, Western Alps). Contrib Mineral Petrol 146(3):341–355

Rubatto D, Schaltegger U, Lombardo B, Colombo F, Compagnoni R (2001) Complex Paleozoic magmatic and metamorphic evolution in the Argenteramassif (Western Alps), resolved with U–Pb dating. Schweiz Mineral Petrogr Mitt 81:213–228

Ruiz-Cruz MD, Sanz de Galdeano C (2017) Genetic significance of zircon in orthogneisses from Sierra Nevada (Betic Cordillera, Spain). Mineral Mag 81(1):77–101

Sanz de Galdeano C, López-Garrido AC (2016) The Nevado–Filábride Complex in the western part of Sierra de los Filabres (Betic Internal Zone). Structure and lithological succession. Boletín Geológico y Minero 127(4):823–836

Sanz de Galdeano C, López-Garrido AC, Santamaría-López A (2016) Major scale structure of the marbles situated between Cóbdar and Macael (Nevado-Filabride Complex, Betic Cordillera, Almería province, Spain), and general stratigraphic arrangement. J Geol Soc Spain 29(2):107–116

Schoene B (2014) U–Th–Pb geochronology. In: Holland HD, Turekian KK (eds) Treatise on geochemistry. Elsevier, Oxford, pp 341–378

Tendero JA, Martín-Algarra A, Puga E, Díaz de Federico A (1993) Lithostratigraphie des métasédiments de l'association ophiolitique Nevado–Filábride (SE Espagne) et mise en évidence d'objets ankéritiques évocant des foraminifères planctoniques du Crétacé: conséquences paléogéographiques. CR Acad Sci Paris 316:1115–1122

Thomson KD, Stockli DF, Clark JD, Puigdefàbrega C, Fildani A (2017) Detrital zircon (U–Th)/(He–Pb) double-dating constraints on provenance and foreland basin evolution of the Ainsa Basin, south-central Pyrenees, Spain. Tectonics 36:1352–1375

Vermeesch P (2012) On the visualization of detrital age distributions. Chem Geol 312–313:190–194

Wu Y, Zheng Y (2004) Genesis of zircon and its constraints on interpretation of U–Pb age. Chinese Sci Bull 49(15):1554–1569